Reversible clustering of gold nanoparticles under confinement

Reversible clustering of gold nanoparticles under confinement

Ana Sánchez-Iglesias, Nathalie Claes, Diego M. Solís, Jose M. Taboada, Sara Bals, Luis M. Liz-Marzán, Marek Grzelczak

Abstract: *A limiting factor of solvent-induced self-assembly of nanoparticles is the need for constant sample dilution in assembly/disassembly cycles. Changes in nanoparticle concentration alter the kinetics of the subsequent assembly process, limiting optical signal recovery. Here we show that by confining hydrophobic nanoparticles in permeable silica nanocapsules, the number of nanoparticles participating in cyclic aggregation remains constant despite bulk changes in the solution, leading to highly reproducible plasmon band shifts at different solvent compositions.*

Control over the spatial distribution of nanoparticles in liquid phase is a convenient strategy for the bottom-up fabrication of dynamic materials.[1,2] In this context, we need stimuli that can drive the assembly/disassembly process. The list of available stimuli keeps constantly increasing, including electromagnetic fields (magnetic field,[3] light[4,5]), temperature[6,7] pH,[8,9] metal ions,[10] (bio)molecules[11,12] or solvent composition.[13–15] The use of the solvent as a stimulus has been proposed by Kumacheva and colleagues,[13] who used hydrophobic polystyrene (PS) capping agents to provide colloidal stability to nanoparticles in tetrahydrofuran (THF), N.N-dimethylformamide (DMF) or dioxane. Addition of water resulted in a self-assembly process driven by hydrophobic forces.[16] Despite of the wide variety of experimental examples, the use of solvents to trigger assembly and disassembly hinders the switching ability, which is however readily achievable by other stimuli, such as light.[4] The reason is that the alternate assembly/disassembly steps require increasing dilution of the sample. The volume changes during subsequent cycles alter the particle concentration and in turn the kinetics of assembly, leading to poor reproducibility. Thus, to ensure control over solvent-induced self-assembly one needs to keep constant the number of nanoparticles involved in the cyclic aggregation, regardless of bulk modifications in solvent composition. Such a scenario remains unachieved in currently available experimental models.

The central hypothesis behind our work involves the confinement of polystyrene-stabilized gold nanoparticles within permeable (mesoporous silica) capsules to fix the number of selfassembling nanoparticles, resulting in highly reproducible shifts of the localized surface plasmon resonance (LSPR). Combination of 3D characterization by electron tomography and numerical simulations allowed us to confirm that the experimentally observed plasmon shifts correlate with optical changes at individual aggregates. **Figure 1** schematically describes the fabrication of permeable capsules carrying hydrophobic gold nanoparticles: (1) PSstabilized gold nanoparticles (in THF) cluster upon addition of water and are subsequently encapsulated within a blockcopolymer micelle. (2) The resulting polymeric micelles are then coated by a rigid shell of mesoporous silica. (3) Block-copolymer molecules are finally removed by resuspending the capsules in THF, yielding hollow capsules filled with hydrophobic nanoparticles.

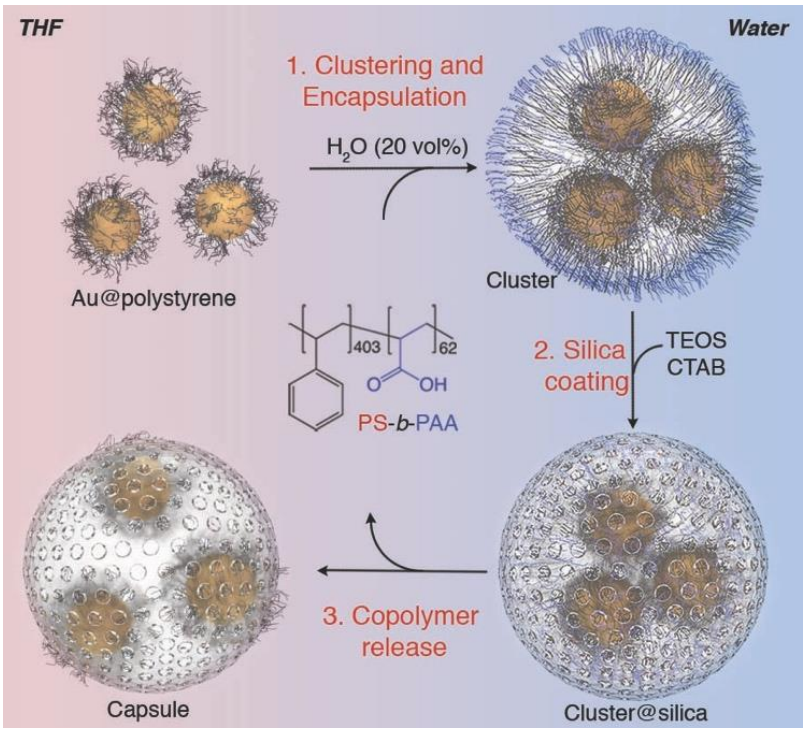

Figure 1. Fabrication of capsules containing Au NP clusters. (1) Polystyrene capped gold nanoparticles aggregate upon addition of water and are encapsulated in polymeric micelles. (2) Mesoporous silica coating of polymerencapsulated clusters. (3) Removal of block-copolymer by resuspersion in THF.

We first synthesized gold nanoparticles (40.8±1.7 nm, **Figures 2 & S1**) capped with benzyldimethylhexadecylammonium chloride (BDAC), which was exchanged with thiolated polystyrene (53 kg/mol).[14] Next we induced clustering and encapsulation of nanoparticles within polymeric micelles, as per our previous work.[17] Typically, addition of water (20 vol%) to colloidally stable polystyrenecoated gold nanoparticles (Au@PS) in THF resulted in aggregation/clustering, which was quenched after 3 minutes by addition of the polymeric surfactant (polystyrene-blockpoly(acrylic acid), PS-*b*-PAA) (**Figure S2**). This process resulted in quasi-monodisperse plasmonic micelles (clusters) (277.2±18.8 nm in diameter), containing 7±2 AuNPs and exhibiting long-term colloidal stability in water. The clusters were then coated with mesoporous silica (20.1±0.7 nm thick), displaying radially oriented pores (~ 4 nm pore thickness) (**Figure 2b,c**). The LSPR band of BDAC-stabilized Au nanoparticles redshifted from 527 to 564 nm upon clustering, accompanied by extinction increase over the entire spectral range, due to significantly increased scattering. Deposition of the silica shell did not affect the LSPR position but caused a slight further increase in extinction (**Figure 2a**).

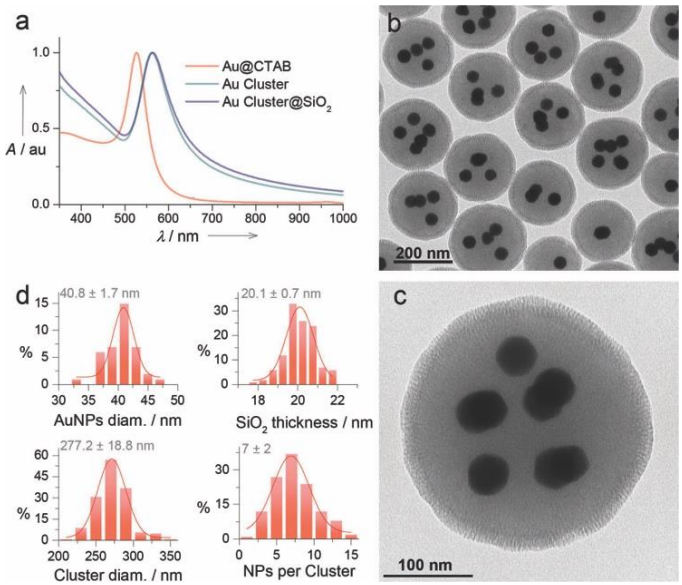

Figure 2. Clustering of nanoparticles. (a) Normalized UV-Vis-NIR spectra of nanoparticles before and after clustering and upon silica coating. All spectra were recorded in water to facilitate comparison. (b,c) TEM images of cluster@SiO2 at different magnifications. (d) Histograms showing the distribution in the diameter of nanoparticles and clusters, as well as in silica shell thickness and number of particles per cluster.

Since silica is known to gradually hydrolyze and dissolve in aqueous solution,[18] we passivated cluster@SiO2 particles by silanization with a silane-terminated poly-ethyleneglycol (Si-PEG, 10000 g/mol, see Supporting Information).[19] This coating led to an increase in hydrodynamic diameter, from 322.3±2.5 to 357.2±2.2 nm, with no change in zeta-potential (-40 mV), and without altering the composition of the polymeric micelle (**Figure S3**). Evaluation of the long-term stability (1 month) of PEGylated cluster@SiO2 in water confirmed the absence of structural and optical changes. On the other hand, resuspension of cluster@SiO2 in THF resulted in the diffusion of block-copolymer molecules into the bulk solution, through the mesoporous silica shell. To gain insight into the kinetics of the process, we monitored copolymer release by UV-Vis-NIR spectroscopy (**Figure 3a**). Extinction was observed to gradually decrease, accounting for decreased scattering, but reached a plateau after two hours. By plotting the absorbance at 400 nm (Abs@400) vs. incubation time, we observed an induction time of 10 min and a subsequent drop in absorbance corresponding to copolymer extraction, which is completed after 2 h (**Figure 3b**). We also observed an LSPR blueshift from 553 to 539 nm (**Figure 3b**), due to a decrease in local refractive index (from 1.59 for polystyrene to 1.40 for THF) and increased interparticle distances. The LSPR maximum of empty capsules in THF had a similar value to that of free Au@PS in the same solvent (**Figure S4**), suggesting that the particles are not aggregated inside the capsule. Time-dependent TEM characterization confirmed gradual block-copolymer extraction through an increase of contrast inside the capsules (**Figure S5**). We also implemented STEM-EDX elemental analysis to visualize the changes in carbon intensity before and after copolymer release, while other elements (Si, O, Au) remained unchanged (**Figure 3c,d**).

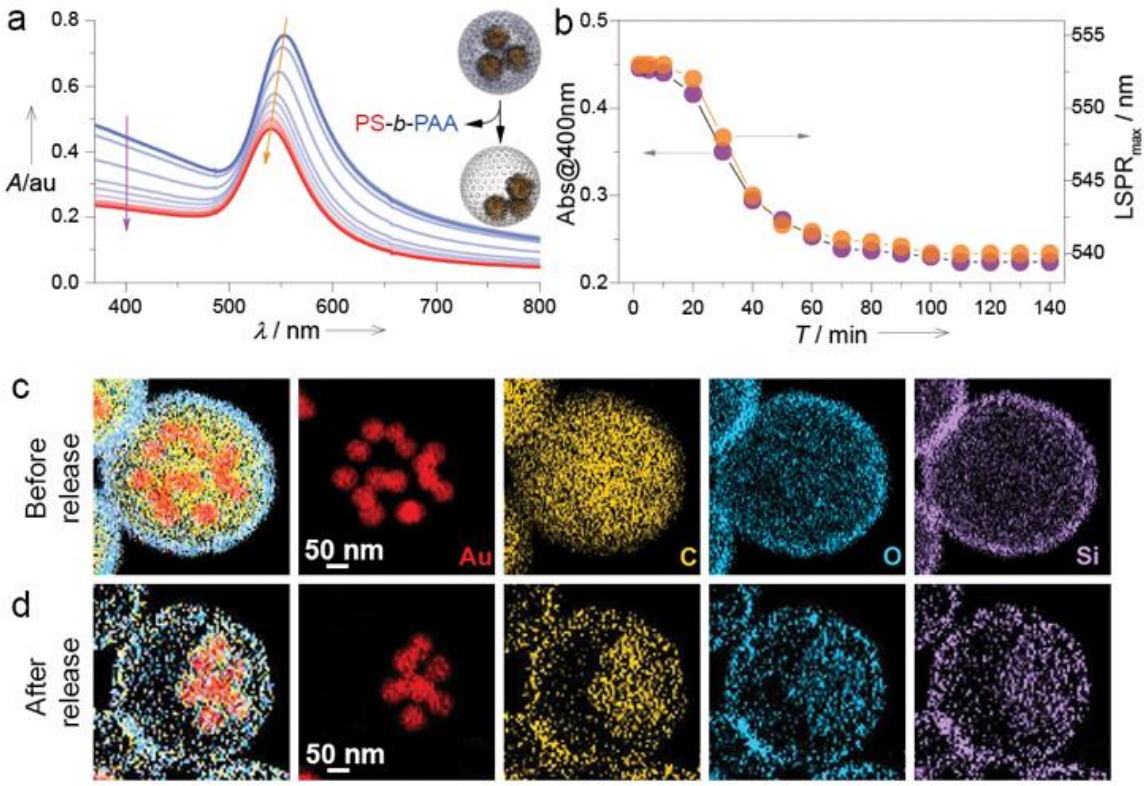

Figure 3. Formation of capsules through block-copolymer extraction. (a) Timedependent UV-Vis-NIR spectra of encapsulated clusters in THF. (b) Changes in absorbance at 400 nm and LSPR maximum during incubation in THF. (c) STEM-EDX elemental analysis of encapsulated clusters (before and after blockcopolymer extraction), showing a decrease in carbon signal.

Reversible aggregation of Au@PS within the capsules was tested by repeated variations in water content. Due to sample dilution in each aggregation step (H2O addition) the initial solvent composition (pure THF) could not be recovered during disassembly (THF addition). Therefore, we defined lower (5 vol%) and upper (40 vol%) limits of water concentration, at which the LSPR would be fully blueshifted (dispersed) and fully redshifted (aggregated), respectively (**Figure S6**). We performed 15 aggregation cycles by alternating the amount of water between 5 and 50 vol% (water excess to ensure full redshift), obtaining highly reproducible spectral features. Not only the LSPR maximum oscillated between 542 and 572 nm with high precision, the full width at half maximum (FWMH) also oscillated between 88 and 155 nm (**Figure 4b**). TEM analysis at the limiting water

contents confirmed the structures expected from the measured optical spectra; Au@PS remained dispersed in the capsules at 5 vol% water, but aggregated at 50 vol% (**Figure 4a**). The exceptional LSPR switching ability arises from a constant number of particles participating in the aggregation process, ~7 for each cluster. We additionally observed that nanoparticle confinement in the capsules results in an increased aggregation rate, as compared to free nanoparticles in solution. Whereas less than 3 min was required to fully redshift the LSPR band in confined nanoparticles, it took nearly 20 minutes to aggregate free Au@PS at the same water content (20 vol%) (**Figure 4f**). This is likely due to the decreased initial interparticle distances under confinement, which allows for faster aggregation.

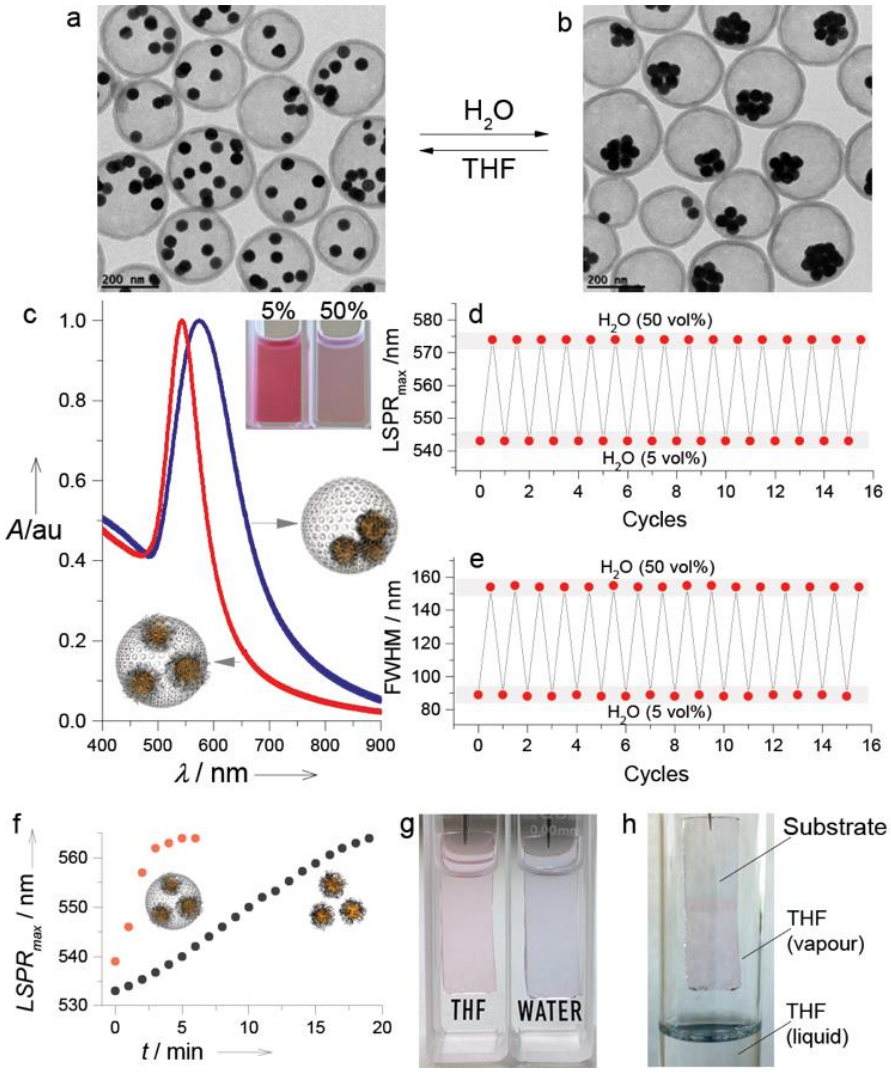

Figure 4. Reversible optical switching. (a,b) TEM images of capsules with low and high water content (a: 5 vol%; b: 50 vol%). (c) UV-Vis-NIR spectra of capsules during cyclic addition of water and THF. (d,e) Evolution of LSPR maxima (d) and FWHM (e) during 15 cycles. (f) Aggregation

kinetics of confined and free Au@PS, at constant nanoparticle concentration and water content (20 vol%). (g) Photographs showing a capsule functionalized glass substrate in THF (red) and in water (blue). (h) Photograph of a capsule-functionalized glass slide exposed to vapor from warm THF, leading to a fast color change.

To further demonstrate the ability of this system to switch its optical response, we immobilized the loaded capsules on a solid (glass) substrate for fast handling in and out of different solvents. Using a conventional layer-by-layer method,[20] we functionalized a glass slide with a cationic polyelectrolyte, followed by immobilization of capsules through electrostatic interactions. A single layer of capsules was enough to impose a visible coloration to the glass. Cyclic immersion of the substrate in THF and water produced optical changes that were readily detected by the naked eye and confirmed by spectral shifts (**Figure 4g and S7**). Note that during execution of these experiments the humidity in our laboratory was 80% (conditioned by weather in Donostia-San Sebastian in mid-August), so the particles remained aggregated when stored in solution-free conditions. Exposure of the supported capsules to THF vapor led to an immediate color change from blue to red, as a result of the THF-rich atmosphere (**Figure 4h**). Videos demonstrating color switching of a glass slide are provided as Supporting Information (**Movie S1** and **Movie S2**). Facile handling of the substrate and reproducible optical response pave the way toward the design of colorimetric sensors for humidity, volatile solvents, or small hydrophobic molecules.

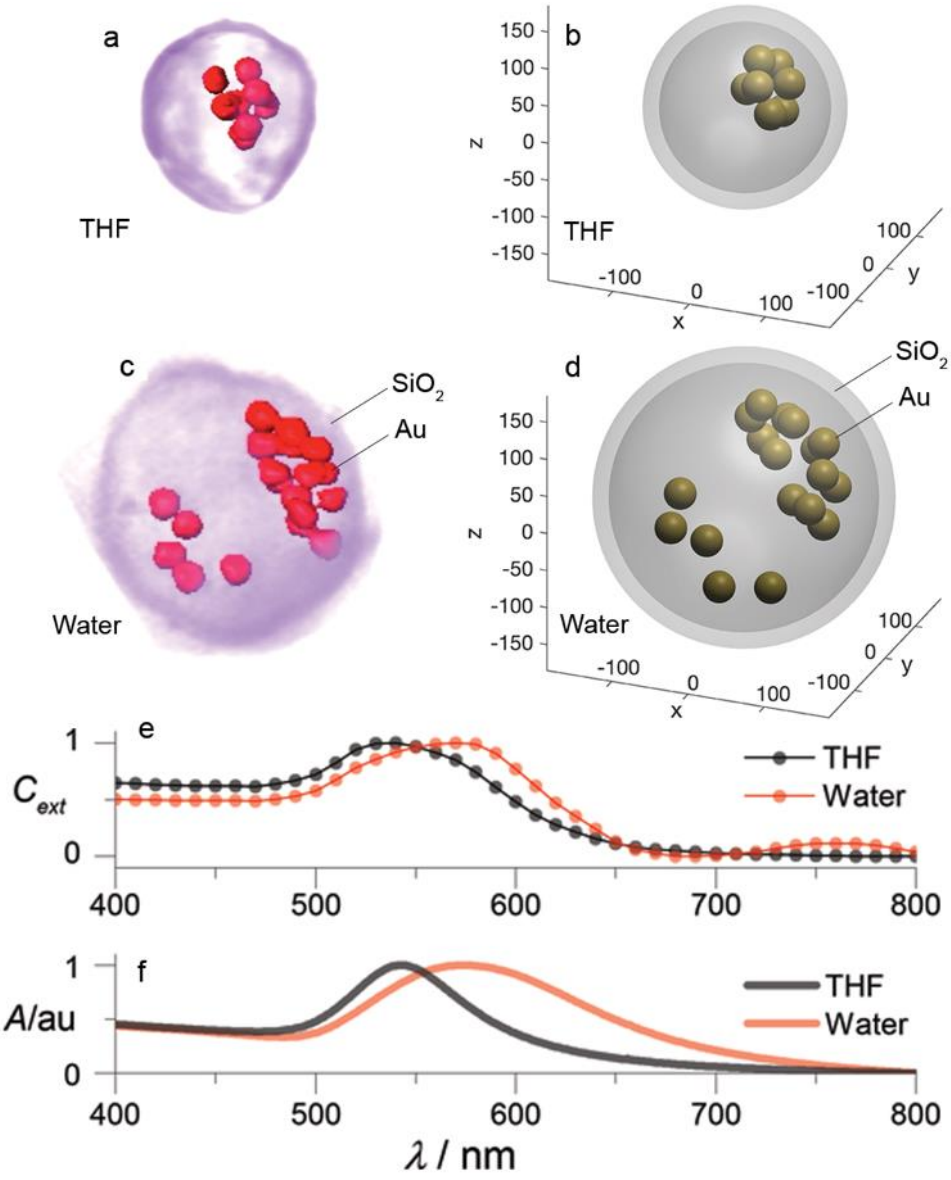

Figure 5. Numerical simulation of LSPR shift. (a,c) 3D electron tomography rendering of randomly selected capsules in water (a) and in THF (c). (b,d) 3D models constructed from the coordinates obtained by 3D electron tomography. The models served as an input for numerical calculation of spectra. (e) Calculated extinction spectra of clusters in THF and in water. (f) Experimental spectra, showing good correlation of LSPR positions.

Reversible assembly involves in this case seven nanoparticles on average, thereby resulting in highly reproducible

plasmon shifts. As a consequence, the LSPR shift at the level of individual capsules is expected to reflect the LSPR shift in the bulk sample. Therefore, numerical simulation of the spectral changes for

dispersed and aggregated particles inside a capsule should faithfully reproduce the experimental optical changes. We employed 3D electron tomography to acquire an accurate representation of the spatial distribution of Au@PS at randomlyselected capsules containing both aggregated and dispersed nanoparticles, at specific solvent compositions (**Figure 5a** and **Movies S3 and S4** in SI). Accurate 3D coordinates obtained from 3D electron tomography (3D models in **Figure 5b**) were directly used as input for simulations of extinction spectra by a reported methodology based on surface integral equations with the method of moments formulation.[21] This allows time-effective simulation of arbitrary complex nanostructures (in this case including the nanoparticles at specific positions, the silica shell and the solvent; see SI for details). Even though the selected capsules differed in the overall diameter and the number of Au@PS particles, the obtained numerical extinction spectra accurately resemble the experimental absorbance spectra of the solution in the same solvents. For the simulated spectra in THF, the LSPR maximum was at 538 nm while in water it was at 572 nm, in good agreement with the experimental data (540 nm for THF and 572 nm for water).

Again, such a good correlation between simulated and experimental data is due to an invariant number of particles involved in the aggregation process. It should be noted that numerical spectra confirmed that the presence of the silica shell does not affect the optical response in THF because of the similar refractive indexes of SiO2 (1.47) and THF (1.40). In conclusion, we demonstrated that confinement of gold nanoparticles in permeable silica shells allows for highly reproducible clustering at different solvent compositions, since the number of particles participating in the aggregation process remained constant. Our methodology shows unprecedented optical signal switching during the solvent-induced reversible clustering of nanoparticles. The structural advantage of our method relies on the fact that the nanoparticles are not loaded into the predefined container, but the container is built around as prepared clusters, avoiding issues related to cargo leakage. Incidentally, our method is also cost-efficient since the copolymer can be recovered for subsequent encapsulation processes.

Acknowledgements

L.M.L.-M. and M.G. acknowledge funding from the Spanish MINECO (Grant #MAT2013-46101R). N.C. and S.B. acknowledge financial support from European Research Council (ERC Starting Grant #335078-COLOURATOM). D.M.S., and J.M.T, acknowledge funding from the European Regional Development Fund (ERDF) and the Spanish MINECO (Projects TEC2017-85376-C2-1-R, TEC2017-85376-C2-2-R), and from the ERDF and the Galician Regional Government under agreement for funding the Atlantic Research Center for Information and Communication Technologies (AtlantTIC).

Keywords: nanoparticles • self-assembly • mesoporous silica • plasmon band • tomography

[1] B. A. Grzybowski, K. Fitzner, J. Paczesny, S. Granick, *Chem. Soc. Rev.* **2017**, *46*, 5647–5678.
[2] Z. Nie, A. Petukhova, E. Kumacheva, *Nat. Nanotechnol.* **2010**, *5*, 15–25.
[3] K. Butter, P. H. H. Bomans, P. M. Frederik, G. J. Vroege, A. P. Philipse, *Nat. Mater.* **2003**, *2*, 88–91.
[4] R. Klajn, K. J. M. Bishop, B. A. Grzybowski, *Proc. Natl. Acad. Sci.* **2007**, *104*, 10305–10309.
[5] P. K. Kundu, D. Samanta, R. Leizrowice, B. Margulis, H. Zhao, M. Börner, T. Udayabhaskararao, D. Manna, R. Klajn, *Nat. Chem.* **2015**, *7*, 646–652.
[6] Y. Liu, X. Han, L. He, Y. Yin, *Angew. Chem. Int. Ed.* **2012**, *51*, 6373–6377.
[7] S. Balasubramaniam, N. Pothayee, Y. Lin, M. House, R. C. Woodward, T. G. St. Pierre, R. M. Davis, J. S. Riffle, *Chem. Mater.* **2011**, *23*, 3348–3356.
[8] D. Wang, B. Kowalczyk, I. Lagzi, B. A. Grzybowski, *J. Phys. Chem. Lett.* **2010**, *1*, 1459–1462.
[9] L. Heinen, T. Heuser, A. Steinschulte, A. Walther, *Nano Lett.* **2017**, *17*, 4989-4995.
[10] S. Si, M. Raula, T. K. Paira, T. K. Mandal, *ChemPhysChem* **2008**, *9*, 1578–1584.
[11] K. L. Gurunatha, A. C. Fournier, A. Urvoas, M. Valerio-Lepiniec, V. Marchi, P. Minard, E. Dujardin, *ACS Nano* **2016**, *10*, 3176–3185.
[12] G. von Maltzahn, D.-H. Min, Y. Zhang, J.-H. Park, T. J. Harris, M. Sailor, S. N. Bhatia, *Adv. Mater.* **2007**, *19*, 3579–3583.
[13] Z. Nie, D. Fava, E. Kumacheva, S. Zou, G. C. Walker, M. Rubinstein, *Nat. Mater.* **2007**, *6*, 609–614.
[14] A. Sánchez-Iglesias, M. Grzelczak, T. Altantzis, B. Goris, J. Pérez- Juste, S. Bals, G. Van Tendeloo, S. H. Donaldson, B. F. Chmelka, J. N. Israelachvili, et al., *ACS Nano* **2012**, *6*, 11059–11065.
[15] H. Hu, F. Ji, Y. Xu, J. Yu, Q. Liu, L. Chen, Q. Chen, P. Wen, Y. Lifshitz, Y. Wang, et al., *ACS Nano* **2016**, *10*, 7323–7330.
[16] R. M. Choueiri, A. Klinkova, H. Thérien-Aubin, M. Rubinstein, E. Kumacheva, *J. Am. Chem. Soc.* **2013**, *135*, 10262–10265.
[17] M. Grzelczak, A. Sánchez-Iglesias, L. M. Liz-Marzán, *CrystEngComm* **2014**, *16*, 9425–9429.
[18] H. Yamada, C. Urata, Y. Aoyama, S. Osada, Y. Yamauchi, K. Kuroda, *Chem. Mater.* **2012**, *24*, 1462–1471.
[19] V. Cauda, C. Argyo, T. Bein, *J. Mater. Chem.* **2010**, *20*, 8693–8699.
[20] I. Pastoriza-Santos, A. Sánchez-Iglesias, F. J. García de Abajo, L. M. Liz-Marzán, *Adv. Funct. Mater.* **2007**, *17*, 1443–1450.
[21] D. M. Solís, J. M. Taboada, F. Obelleiro, L. M. Liz-Marzán, F. J. García de Abajo, *ACS Nano* **2014**, *8*, 7559–7570.